Available online at www.sciencedirect.com
SCIENCE DIRECT®
Journal of Power Sources 136 (2004) 1–9
JOURNAL OF POWER SOURCES
www.elsevier.com/locate/jpowsour

Three-dimensional numerical analysis of proton exchange membrane fuel cells (PEMFCs) with conventional and interdigitated flow fields

Guilin Hu, Jianren Fan*, Song Chen, Yongjiang Liu, Kefa Cen

Institute for Thermal Power Engineering and CE&EE, Zhejiang University, Hangzhou 310027, PR China

Received 14 July 2003; received in revised form 20 April 2004; accepted 6 May 2004

Available online 4 July 2004

Abstract

A three-dimensional, steady-state mathematical model is described to investigate the fluid flow, species transport and electrochemical reaction in the PEM fuel cells with conventional and interdigitated flow fields. The multidimensional characteristics of flow, species and current distributions are computed by method based on volume-control finite-discrete technique. After comparing the absolute value of convective and diffusion component of oxygen flux quantitatively, we found that forced convection transport mechanism is dominant for the interdigitated flow field design, however the diffusion transport is dominant for the conventional flow field design. The performance and the pressure loss of these two different designs are calculated and compared; results show that interdigitated flow field design have better performance for its advantage in mass-transport ability, however have larger pressure loss for its flow through the electrode. Finally, experimental results reported in the literature and predicted polarization curves are compared to evaluate the numerical model employed.

Keywords: Proton exchange membrane fuel cell; Conventional flow field; Interdigitated flow field; Numerical modeling

1. Introduction

The proton exchange membrane fuel cell (PEMFC) engines, using polymer membrane as electrolyte, are considered to be promising power sources, especially for transportation applications. This fuel cell has many important attributes such as high efficiency, clean, quiet, low temperature operation, capable of quick start-up, no liquid electrolyte and simple cell design. However, before this system becomes competitive with the traditional combustion engine, its performance and costs must be further optimized. In order to enhance its performance, a new flow field design called the interdigitated flow field has been developed and proven to be very effective by experiment [1–3], as schematically shown in Fig. 1b. Comparing to flowing over the surface of the electrodes in the conventional parallel-channel flow field shown in Fig. 1a, these interdigitated flow fields in effect have converted the transport of the reactant/product gases to/from the catalyst layers from a diffusion dominated mechanism to a forced convection dominated mechanism by forcing the reactant gases to flow into the electrode in order to exit. The transport rate of the reactive gases to the catalytic reaction layer is enhanced and the electrode-flooding problem in the cathode is reduced, thus increasing the current density at a given cell potential and the limiting current density significantly.

In the last decade a number of one- and two-dimensional mathematical models [4,5] have been presented to investigate PEM fuel cells with conventional flow field and their performance. These models cannot account for effect of the flow channel width on the velocity distributions and the species distributions. More recently, three-dimensional models [6,7] based on the computational fluid dynamics approach have been presented and computed by commercial software such as FLUENT and CFX. However, for the interdigitated flow field design, some studies focusing on developing two-dimensional mathematical model [8,9] have been conducted to delineate the flow and transport mechanism. These two-dimensional models cannot consider the composition changes along the flow path, thus their applicability is limited. Um et al. [10] carried out a three-dimensional computational study for PEM fuel cells with conventional and interdigitated flow fields. Fully three-dimensional analysis of transport and reaction in PEM fuel cells with the interdigitated flow field was presented.

* Corresponding author. Tel.: +86 571 8795 1764; fax: +86 571 8799 1863.
E-mail address: fanjr@mail.hz.zj.cn (J. Fan).

0378-7753/$ – see front matter © 2004 Elsevier B.V. All rights reserved.
doi:10.1016/j.jpowsour.2004.05.010

Nomenclature

C	molar concentration, mol cm^{-3}
C_f	fixed charge concentration, mol cm^{-3}
D	diffusion coefficient, cm^2 s^{-1}
F	Faraday constant = 96487 C/mol
H	cell height, cm
I	mean current density, A cm^{-2}
J	transfer current density, A cm^{-3}
k_p	hydraulic permeability, cm^2
k_ϕ	electrokinetic permeability, cm^2
L	catalyst layer width, cm
N	component number and electron number participating in the electrochemical reaction
P	pressure, atm
R	gas constant and production/consumption rate of material
S	stoichiometric coefficient
T	cell temperature, K
u	velocity vector, cm s^{-1}
z_f	fixed site charge

Greek letters

α	transfer coefficient
γ	concentration parameter
ε	porosity of the porous media material
μ	fluid viscosity, kg cm^{-1} s^{-1}
ρ	density of the fluid, mol cm^{-3}
σ	conductivity, Ω^{-1} cm^{-1}
φ	potential, V

Superscripts

eff	effective value

Subscripts

a	anode
c	cathode
f	membrane species (the fixed charge site species)
k	component
m	membrane
ref	reference

The major objective of this work is to develop a three-dimensional model for the simulation of PEMFCs, which can be applied to investigate the multidimensional distributions of current densities, reactants concentrations in the fuel cell with the interdigitated and conventional flow fields, knowledge the fuel cell work principles and mass-transport schemes of these two cell design in more detail. At the end, polarization characteristics for conventional and interdigitated flow fields are predicted and compared. Estimated and experimental results in the published literature were compared to verify the mathematical model used in this paper, reasonable agreement was achieved. In this first step, water transport in the membrane electrode assembly is not modeled in detail. The effect of relative humidity of reactant gases on the performance, and the two-phase phenomena under high current density, is not discussed in this paper, which will be considered in the future work.

2. Mathematical model

The scheme of a PEMFC is shown in Fig. 1. Fig. 1a and b is flow path structure for the conventional and interdigitated flow fields, respectively. For the conventional flow field, two flow channels around the current collector are same, the gas mixture flows in from the inlet, and flows over the electrode surfaces in parallel, and then out from the outlet. For the interdigitated flow field, however, two flow channels around the current collector have a dead-end, which force the gas mixture flow into the backing layers, and then flow out from the outlet of the outlet channel. The common PEM fuel cell can be divided into seven segments across the fuel cell, as illustrated in Fig. 1c. The two outer segments are graphite-plate current collectors with flow channels for reactants and products to enter and exit the cell, respectively. The adjacent segments are electronically conducting porous backing layers that allow for even distribution of reactants to the anode and cathode. The centric polymer membrane spatially separates the fuel cell. The catalyst layers between the membrane and the backing layers are domain for electrochemical reactions. The catalyst layers provide electron, proton and reactants channels. In this work, the computational domain consists of three-dimensional complete fuel cell.

The assumptions used in developing the model are:

1. The gas mixture is incompressible, ideal fluid.
2. The flow in fuel cell is laminar everywhere.
3. The effective diffusion coefficient of reactant gases in the porous media is constant.
4. Isothermal conditions.
5. The diffusion layer, catalyst layer and membrane are isotropic and homogeneous, characterized by effective permeability and uniform porosity.
6. Butler–Volmer kinetics governs the electrochemical reaction.
7. The water produced by electrochemical reaction at the cathode side is in vapor state.
8. The membrane is impervious for reactants gases.

The governing equations are identical for both conventional and interdigitated flow fields, which will be described in the following section. Assuming that the fuel cell is repeated periodically along y-direction, in order to save the computation source and computation time, we take one current collector, half of two flow channels around which as computation domain, illustrated in Fig. 1.

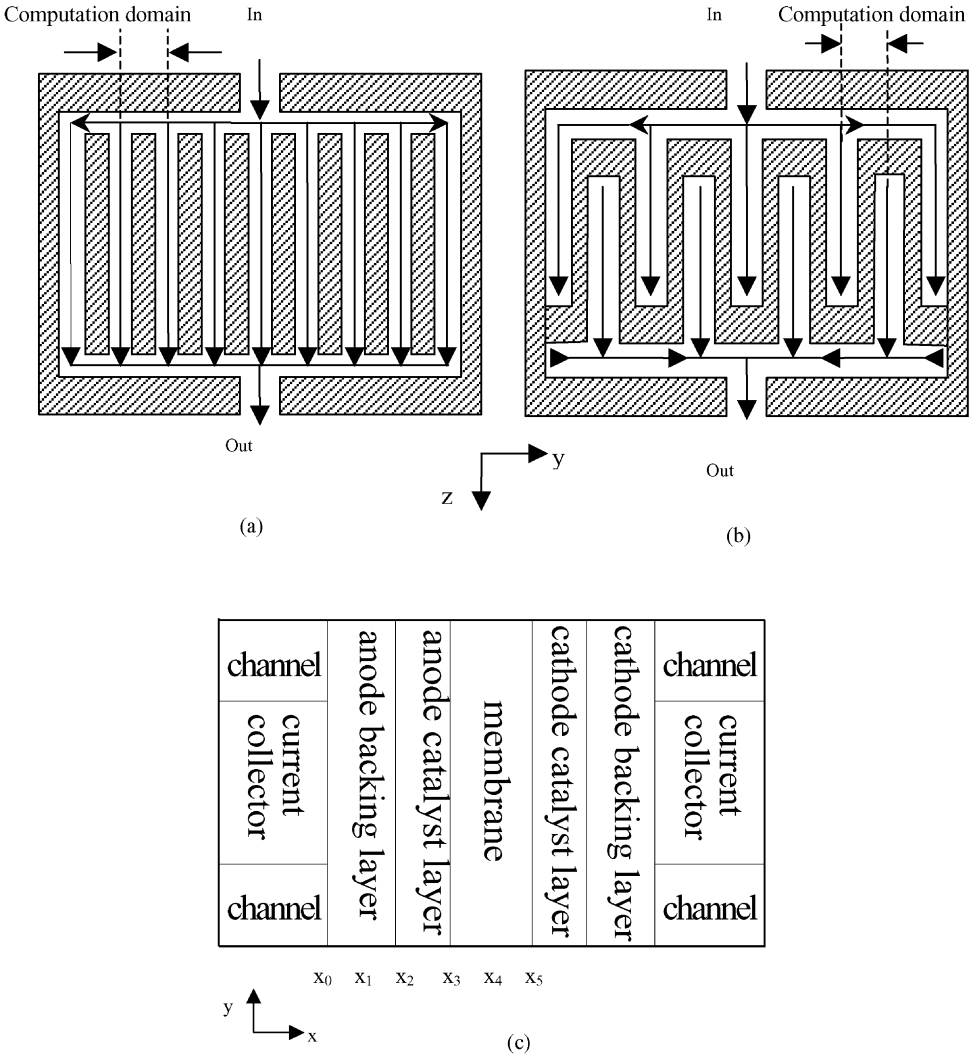

Fig. 1. Schematic of the flow fields structure and the computation domain for a conventional flow field (a) and interdigitated flow field (b). (c) A typical cross-section of the domain and the locations of different layers.

2.1. Continuity equation

The conservation of mass equation for the gas mixture

$$\nabla(\varepsilon\rho\boldsymbol{u}) = S_{\mathrm{m}} \tag{1}$$

where ε is the porosity of the porous media, which is equal to unit for the gas channels, ρ the density, and $\boldsymbol{u}$ the intrinsic fluid velocity vector, $\varepsilon\boldsymbol{u}$ reflects the superficial velocity in the porous media. S_{m} denotes the mass source term considering the electrochemical aspects of the fuel cell, thus they are zero in most of the computation domain except for the activated reaction sites as the anode and cathode catalyst layers. These terms corresponding to the consumption of hydrogen and oxygen in the anode and the cathode, and the production of water in the cathode can be determined as following:

$$S_{\mathrm{m}} = \sum_{k} S_k \tag{2}$$

where S_k stands for the source/sink term of the k'th species induced by the electrochemical reaction occurred in the active catalyst layers.

2.2. Momentum conservation

The fluid flow in the fuel cell can be described by the general equation as:

$$\nabla(\varepsilon\rho\boldsymbol{u}\boldsymbol{u}) = -\varepsilon\nabla p + \nabla(\varepsilon\mu^{\mathrm{eff}}\nabla\boldsymbol{u}) + S_{\mathrm{u}} \tag{3}$$

where p denotes the pressure, μ^{eff} the effective viscous coefficient. Because the fluid flowing in the channels, backing layers and catalyst layer, membrane is different, gas mixture and liquid, so, μ^{eff} stand for gas viscous coefficient for gas mixture in the channel and backing layer, and liquid viscous coefficient for liquid in the catalyst layer and membrane. Furthermore, mass-weighted mixing law gives viscosity of the gaseous mixture. The momentum source S_{u} is used to describe the Darcy's drag force exerted by the

fluid on the solid surface in the porous electrode, catalyst layer and membrane. For the fluid flow in the gas channel, the equation becomes the Navier–Stokes equation. The momentum conservation in the porous media can be reduced to the well-known Darcy's law because the inertia and viscous terms is so small, and can be neglected. However, the macroscopic velocity changes rapidly at the interface between the channel and gas diffusion layer, the macroscopic viscous force and inertial force must be considered in the momentum equation. So, a general equation with appropriate source terms [11] is more suitable for describing the flow in the whole fuel cell. The momentum source terms for different layers can be as [12].

$$S_u = \begin{cases} 0 & \text{gas channel} \\ -\dfrac{\mu^{\text{eff}}}{k}\varepsilon^2 u & \text{backing layer} \\ -\dfrac{\mu^{\text{eff}}}{k_p}\varepsilon_m\varepsilon_{mc}u + \dfrac{k_\phi}{k_p}z_f c_f F\nabla\varphi_m & \text{catalyst layer} \\ -\dfrac{\mu^{\text{eff}}}{k_p}\varepsilon_m u + \dfrac{k_\phi}{k_p}z_f c_f F\nabla\varphi_m & \text{membrane} \end{cases} \tag{4}$$

Where φ_m stands for the phase potential of the electrolyte membrane, ε_m is membrane porosity and ε_{mc} is the volume fraction of the membrane phase in the catalyst layer. k is permeability of the backing layer. k_p, k_ϕ stand for the hydraulic permeability and electrokinetic permeability. z_f, c_f are fixed site charge and fixed charge concentration. This equation represents a generalized Darcy equation for the backing layer, and a generalized form of Schlögl's equation for the catalyst layer and membrane.

2.3. Species conservation equations

The species conservation equation for the gas mixture is

$$\nabla(\varepsilon \boldsymbol{u} C_k) = \nabla(D_k^{\text{eff}}\nabla C_k) + S_k \tag{5}$$

Here, k denotes chemical species that include hydrogen, oxygen, nitrogen and water. D_k^{eff} is the effective diffusion coefficient. The S depending on the transfer current can be described as following:

$$S_k = \begin{cases} -\dfrac{j_a}{2F} & \text{for } H_2 \\ \dfrac{j_c}{4F} & \text{for } O_2 \\ -\dfrac{j_c}{2F} & \text{for } H_2O \end{cases} \tag{6}$$

where j stands for the transfer current density, which can be calculated by the following Butler–Volmer kinetics expression:

$$j_a = j_{a,\text{ref}}\left(\frac{C_{H_2}}{C_{H_2,\text{ref}}}\right)^{\gamma_a} \times \left[\exp\left(\frac{\alpha_a}{RT}F\eta_{act}\right) - \exp\left(-\frac{\alpha_c}{RT}F\eta_{act}\right)\right] \tag{7}$$

$$j_c = -j_{c,\text{ref}}\left(\frac{C_{O_2}}{C_{O_2,\text{ref}}}\right)^{\gamma_c} \times \left[\exp\left(\frac{\alpha_a F}{RT}\eta_{act}\right) - \exp\left(-\frac{\alpha_c F}{RT}\eta_{act}\right)\right] \tag{8}$$

where η_{act} the surface overpotential, is defined as:

$$\eta_{act} = \varphi_{a,c} - \varphi_m - V_{oc} \tag{9}$$

where $\varphi_{a,c}$ and φ_m denote the potentials for the carbon phase and membrane phase, respectively, at the catalyst layer. V_{oc} is the reference open-circuit potential of the electrode.

2.4. Potentials

The electrical potentials of the membrane phase φ_m and carbon phase φ_a, φ_c are introduced following the concept of mean parameters. These two types of potentials govern the motion of protons and that of electrons, respectively. Taking local electro-neutrality into account, the electronic current and ionic current produced or consumed in the catalyst layers lead to a voltage drop via Ohm's law according to:

$$i = \pm\sigma\nabla\varphi \tag{10}$$

The governing equation for each sort of current follows the current conservation:

$$\nabla i = j \tag{11}$$

Thus, the three potentials obey the following equations:

$$\nabla(\sigma_m\nabla\varphi_m) = \begin{cases} -j_a, & x_1 < x \le x_2 \\ 0 & x_2 < x < x_3 \\ j_c, & x_3 \le x < x_4 \end{cases} \tag{12}$$

$$\nabla(\sigma_a\nabla\varphi_a) = \begin{cases} 0 & x < x_1 \\ j_a & x_1 \le x < x_2 \end{cases} \tag{13}$$

$$\nabla(\sigma_c\nabla\varphi_c) = \begin{cases} -j_c, & x_3 < x \le x_4 \\ 0, & x_4 < x \end{cases} \tag{14}$$

After obtaining the phase potentials, the current density in the external circuit I can be calculated by the following expression:

$$I = \frac{1}{H} \times \frac{1}{L} \times \int_0^H \int_0^L \left(\sigma_m \frac{\partial\varphi_m}{\partial x}\Big|_{x=x_3}\right) \mathrm{d}y\mathrm{d}z \tag{15}$$

where H is the height of the catalyst layer, L the length. As $\varphi_a|_{x=x_0}$ is taken to be zero, then $\varphi_c|_{x=x_5} - \varphi_a|_{x=x_0} = \varphi_c|_{x=x_5}$ gives total voltage of the whole fuel cell.

2.5. Boundary conditions

The computational domain covers a part of the cell assembly, which is repeated periodically along y-direction. Therefore, on the bottom and top ends ($y = 0$ and $y = H$) periodic boundary conditions for all variables are imposed: $f|_{y=0} = f|_{y=H}$, where f stands for all potentials, concentrations, and velocity.

Boundary condition corresponding to membrane phase potential equation is zero flux along all boundaries of the computational domain, giving Von Neumann boundary condition $\partial\varphi_m/\partial n = 0$. In the current collector the carbon phase potentials are fixed ($\varphi_a^0 = 0$, φ_c^0). Solution of the problem for a given φ_c^0 provides the mean current density in the fuel cell, i.e. a point on the I–V curve. The electron current does not flow to the gas channel and the membrane, the normal component of electron current at the channel surfaces is zero: $\partial\varphi_{a,c}/\partial x = 0$. And the same condition is imposed on both sides of the membrane.

As the membrane/catalyst interface is assumed to be impermeable to gases, the flux of gases is zero at this interface $\partial C_k/\partial x = 0$. The same condition is imposed on surfaces of metal electrodes.

At the inlets, the fluid is supposed to flow into the channel at a known velocity, and the species concentrations are known. Thus, the following Dirac boundary conditions are prescribed:

$$U = U_{in}, \quad V = W = 0, \quad C_k = C_{k,in}$$

At the outlets, the fully developed conditions are applied to velocity and species concentration fields.

2.6. Numerical procedures

The conservation equations, including mass, momentum, species and charges, were converted to a finite-difference form by the control volume method. An orthogonal nonuniform grid for computational discretion was employed in this work. The flow channels of anode and cathode are divided into $12\times20\times360$ equally sized grid cells. The y–z planes of backing layer, catalyst layer and membrane are divided into 40×360 grids, however, in the x-direction through the cell, backing layers are equally divided into four parts, catalyst 2 and membrane 4. The solutions of the velocity component equations are obtained in a staggered control volume. The SIMPLEC (semi-implicit method for pressure-linked equations consistent) scheme was adopted for the pressure correction. The species equations are calculated following the velocity vector, coupled with calculation of the potentials by electrochemical reaction kinetics. The unified domain method was adopted for the coding in this work; we use proper boundary for the parameters, rather than boundary conditions for the dependent variables at the interface between different layers [13]. The coupled set of equations was solved iteratively until the relative error in each field achieved the specific convergent standard (usually10^{-5}).

3. Results and discussions

The results presented below were obtained for the parameters and base conditions listed in Table 1, which is obtained mainly from Bernardi et al. [14].

Fig. 2 illustrates two-dimensional velocity vectors in the cathode x–y plane at $z = L/2$ for both conventional and interdigitated flow fields. It can be seen that the magnitude of velocity in the interdigitated flow field is one or two orders larger than that in the conventional flow field. Fig. 2a shows the velocity vectors in the conventional flow field, these velocities are pointing downward from the membrane to the cathode channel. It is because that in the cathode oxygen consumed on the membrane surface is less than the water vapor produced on the membrane surface. Fig. 2b displays the velocity field in the interdigitated flow field. It is evident that there exist bypass flow around the current collector shoulder and also strong forced convection along the reaction surface. The flow from the inlet channel to the outlet channel can enhance providing the reactants to the catalyst layers and removing the products from the catalyst layers. Thus, the performance of the fuel cell can be improved essentially, especially at higher current density.

Table 1
Physical parameters and base conditions

Quantity	Value
Operating temperature (°C)	80
Pressure of anode channel (atm)	1
Pressure of cathode channel (atm)	1.5
Length of the channel, L (cm)	6.0
Channel height (cm)	0.05
Fuel cell height (cm)	0.2
Channel width (cm)	0.07
Backing layer width (cm)	0.024
Catalyst layer width (cm)	0.006
Membrane width (cm)	0.025
α_a	0.5
α_c	1.0 [16]
γ_a	0.5
γ_c	1.0
Hydraulic permeability of membrane, k_p (cm^2)	1.8×10^{-14}
Permeability of backing layer, k (cm^2)	1.76×10^{-7}
Electrokinetic permeability, k_ϕ (cm^2)	7.18×10^{-16}
Hydrogen mole fraction at the inlet of the cathode	1.0
Membrane porosity, ε_m	0.5
Volume fraction of membrane in the catalyst layer, ε_{mc}	0.5
Porosity of the backing layer, ε_0	0.5
Membrane phase conductivity, σ_m (Ω^{-1} cm^{-1})	0.034
Carbon phase conductivity, $\sigma_{a,c}$ (Ω^{-1} cm^{-1})	40
Fixed charge concentration, C_f (mol cm^{-3})	1.2×10^{-3}
Oxygen mole fraction at the inlet of the cathode	0.21
Nitrogen mole fraction at the inlet of the cathode	0.79
Reference transfer current density at anode, $j_{a,ref}$ (A cm^{-3})	5.0×10^2
Reference transfer current density at cathode, $j_{c,ref}$ (A cm^{-3})	4.4×10^{-4}
Velocity at the inlet (cm s^{-1})	50

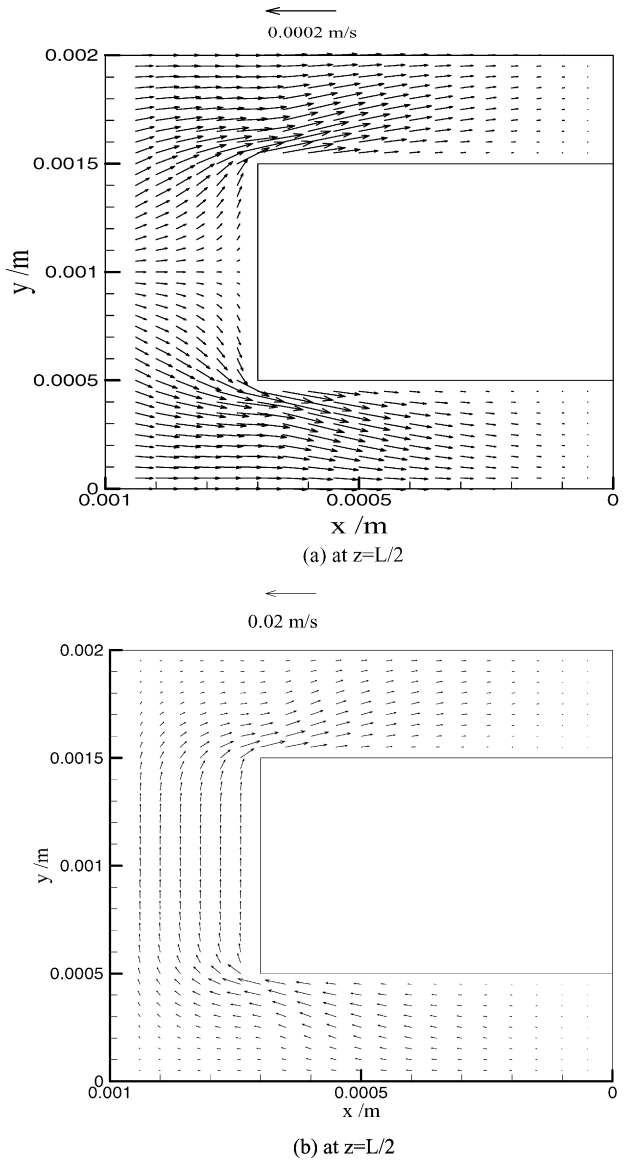

Fig. 2. Two-dimensional velocity fields in the cathode x–y plane cross-backing layer and flow channels at $z = L/2$ for $V_{cell} = 0.7$ V: (a) conventional flow field; (b) interdigitated flow field.

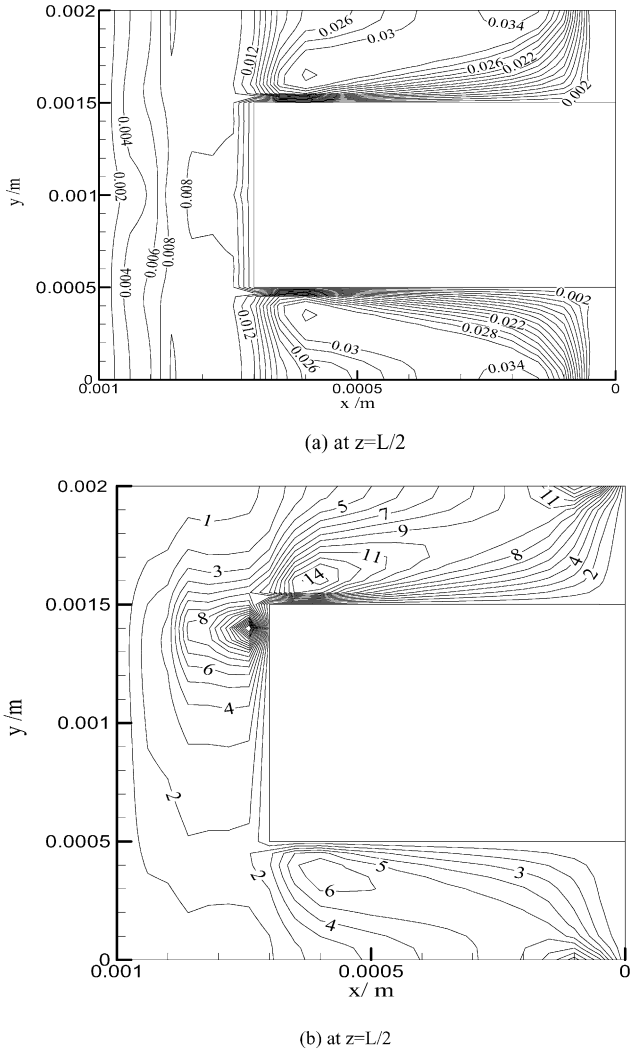

Fig. 3. Ratios f_D/f_c of absolute values of diffusion $f_D = |D\nabla C|$ and convective $f_c = |\varepsilon uC|$, components of oxygen flux in the cathode x–y plane at $z = L/2$ for $V_{cell} = 0.7$ V: (a) conventional flow field; (b) interdigitated flow field.

According to species transport equation 5, the species flux is supported by two processes: convection and diffusion. Fig. 3 shows the ratio of both absolute components of the flux of the oxygen in the cathode x–y plane at $z = L/2$ for the conventional and interdigitated flow fields. It is seen that in the conventional flow field the convection term, $|\varepsilon \boldsymbol{u} C|$, is two or three order less than the diffusion term, $|D\nabla C|$, the reactants is mainly transported by the diffusion mechanism, as displayed in Fig. 3a. This is because that the velocity for the conventional flow field is very small, however, the gradient of concentration is higher. However, for the interdigitated flow field, the forced flow enhance convection flux in the diffusion layer, the convection term take more important effect to the transport process, and enhance the gas mixture transport, as shown in Fig. 3b. It also indicates those interdigitated flow fields effectively convert the transport of the reactant or product gases to or from the catalyst layers from a diffusion mechanism to a forced convection mechanism.

Fig. 4 shows the water vapor mole fraction in the y–z plane at the interface between the cathode catalyst layer and the porous backing layer for the conventional and interdigitated flow fields. From Fig. 4a, in the conventional flow field, the water vapor distribution is symmetric around the centerline in z-direction for the same flow in the channel, and increase along the channel for the electrochemical reaction. In the interdigitated flow field, however, maximum water vapor concentration appears in the outlet portion of the outlet channel, because the flow from inlet channel into electrode, and out from the outlet channel, as illustrated in Fig. 4b.

Fig. 5 displays the local current density distribution in the cathode catalyst layer (in the y–z plane) with voltage 0.7 V

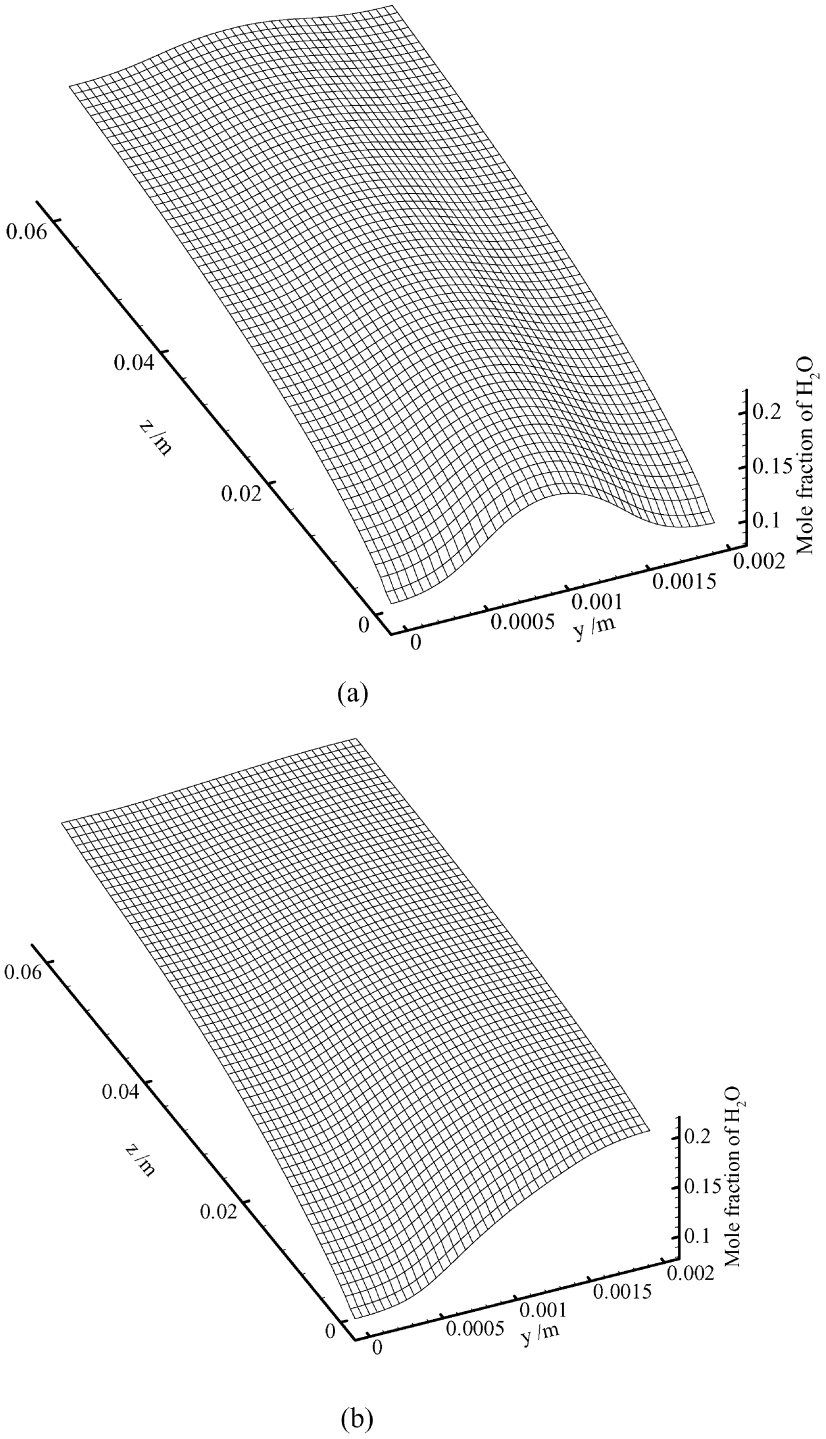

Fig. 4. Water mole fraction distributions at the interface between the catalyst layer and the membrane for $V_{cell} = 0.7$ V: (a) conventional flow field; (b) interdigitated flow field.

for the conventional and interdigitated flow fields. The local current density has similar trends because it depends on the oxygen amount transported to the catalyst layer. Fig. 5a shows the local current density distribution in the conventional flow field. The current density distribution, which is controlled by oxygen diffusion, is symmetric around the centerline in *z*-direction for the same flow in the channel. The local current density in the front of the current collector is smaller than that in front of the channel, because the limitation of the diffusion, the reaction surface cannot be applied fully. The current density in the interdigitated flow field is controlled by forced convection, shown in Fig. 5b. Near the entrance of the flow channel in the interdigitated flow field, the local current density is higher because the

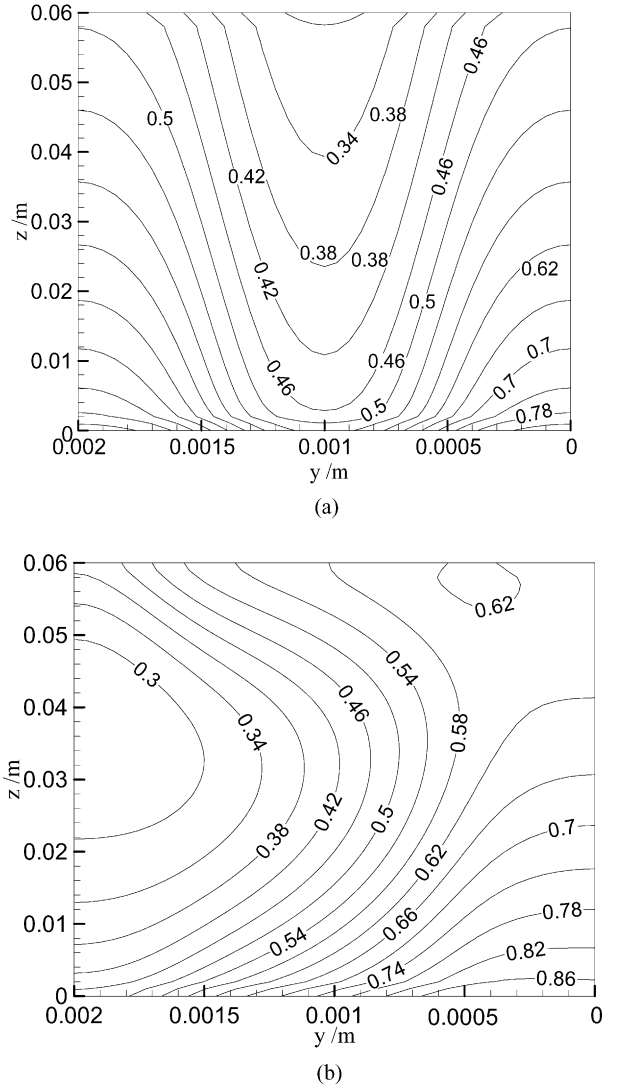

Fig. 5. Local current density distributions in the y–z plane for $V_{cell} = 0.7$ V: (a) conventional flow field; (b) interdigitated flow field.

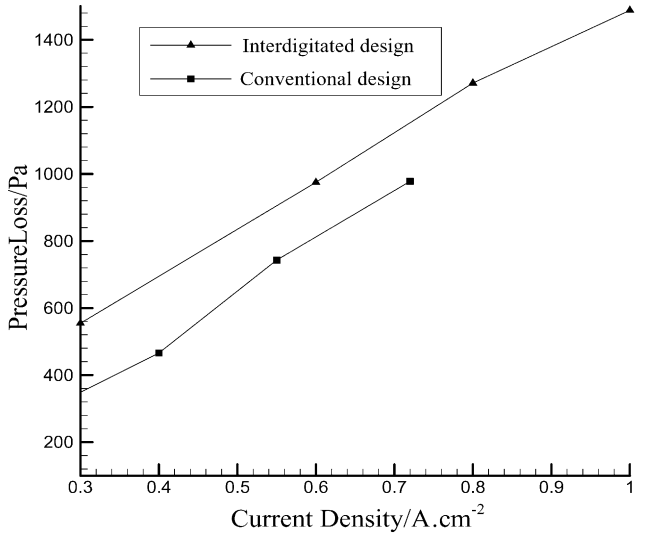

Fig. 6. Pressure drops in the conventional and interdigitated flow fields for different current density.

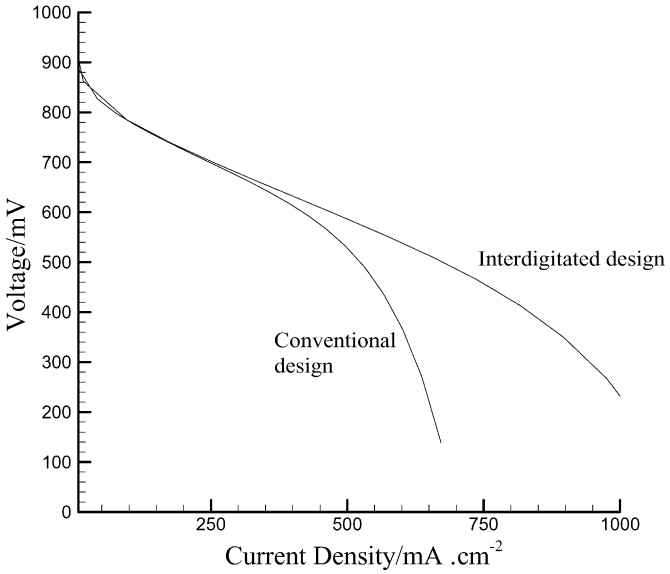

Fig. 7. Comparison of performance of fuel cell with conventional and interdigitated flow fields.

oxygen concentration gradients across the backing layer is larger, followed by diminishing local current density due to the reduced oxygen concentration along the flow channel direction for the electrochemical reaction.

Fig. 6 shows the pressure drop for the conventional and interdigitated flow fields. The interdigitated flow field causes larger pressure drop than the conventional flow field for its fluid flowing through the porous electrode.

The comparison of performance for conventional and interdigitated flow fields is illustrated in Fig. 7. It is obvious that the interdigitated flow field outperforms the conventional flow field, especially at high current densities. The limit current density for a fuel cell with the interdigitated flow field is improved one time corresponding to the fuel cell with the conventional flow field. This is because that high oxygen transfer rate is required to be provided at high current density, which cannot be satisfied by the conventional flow field for the diffusion limitations, whereas can be fulfilled by the interdigitated flow field by strong forced convection.

The availability of our model and its simulation was verified by comparing estimated and experimental polarization curves obtained by Nguyen [15], as displayed in Fig. 8. The numerical model has been run with parameters reported in Table 1 and the conditions similar to experimental case, i.e. temperature is 298.15 K, and pressure is 1 atm. It indicates that the predicted results agree well with experimental data. It should be pointed out that the reference transfer current density was adjusted to achieve the good agreement between the present model predictions and the experimental data. Both the modeling results and the experimental data show the same factor of the fuel cell performance increase when

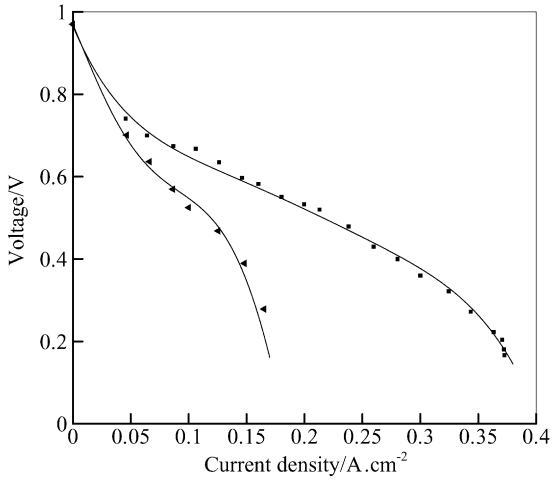

Fig. 8. Comparison between experimental (scattered dots) and estimated polarization curves (full lines): (■) interdigitated flow field; (▼) conventional flow field.

interdigitated flow field is used. Especially, an interdigitated flow field can greatly enhance limiting current density, because mass-transport limitations become main hindrance for performance under high current density.

4. Conclusions

A steady-state, three-dimensional mathematical model was employed to investigate and compare the characteristics of a proton exchange membrane fuel cell with the interdigitated and conventional flow fields. The multidimensional flow structure, distributions of reactants concentrations and current densities for the fuel cell has been calculated. Comparison with a conventional flow fields design fuel cell, an interdigitated flow fields can provide high reactants to catalyst and products from catalyst; enhance limiting current density and polarization performance by forced convectional flow fields through the electrode. However, there have larger pressure drop between the inlet and the outlets in the fuel cell with interdigitated flow field, which may be a main reason hindering interdigitated design application. Polarization curves predicted by numerical modeling compared well with experimental data in the published literature.

Acknowledgements

The authors wish to express their thanks to Natural Science Foundation of Zhejiang Province (PR China, Grant No. 501140).

References

[1] A. Kazim, H.T. Liu, P. Forges, Modeling of performance of PEM fuel cells with conventional and interdigitated flow fields, J. Appl. Electrochem. 29 (1999) 1409–1416.
[2] T.V. Nguyen, Modeling two-phase flow in the porous electrodes of proton exchange membrane fuel cells using the interdigitated flow fields, Presented at the 195th Meeting of Electrochemical Society, 4–7 May 1999, Seattle.
[3] D.L. Wood, J.S. Yi, T.V. Nguyen, Effect of direct liquid water injection and interdigitated flow field on the performance of proton exchange membrane fuel cells, Electrochim. Acta 43 (1998) 3795–3809.
[4] T.F. Fuller, et al., Water and thermal management in solid-polymer-electrolyte fuel cells, J. Electrochem. Soc. 140 (1993) 1218.
[5] V. Gurau, et al., Two-dimensional model for proton exchange membrane fuel cells, AICHE J. 44 (1998) 2410.
[6] S. Dutta, et al., Three-dimensional numerical simulation of straight channel PEM fuel cells, J. Appl. Electrochem. 30 (2000) 135.
[7] T. Berning, et al., Three-dimensional computational analysis of transport phenomena in a PEM fuel cell, J. Power Sour. 106 (2002) 284.
[8] J.S. Yi, T.V. Nguyen, Multicomponent transport in porous electrodes of proton exchange membrane fuel cells using the interdigitated gas distributors, J. Electrochem. Soc. 146 (1999) 38–45.
[9] M. Hu, A. Gu, Y. Shi, Modeling of the cathode of proton exchange membrane fuel cell (PEMFC) using interdigitated flow fields, Chinese J. Power Sour. 26 (2) (2002) 84–88.
[10] S. Um, C.Y. Wang, Three-dimensional analysis of transport and reaction in proton exchange membrane fuel cells, in: Proceedings of the ASME Fuel Cell Division, 5–10 November 2000, Walt Disney World Dolphin, Orlando.
[11] R. Bird, et al., Transport Phenomena, Wiley, New York, 1960.
[12] S. Um, C.Y. Wang, K.S. Chen, Computational fluid dynamics modeling of proton exchange membrane fuel cells, J. Electrochem. Soc. 147 (12) (2000) 4485–4493.
[13] S.V. Patankar, Numerical Heat Transfer and Fluid Flow, Hemisphere, New York, 1980.
[14] D.M. Bernardi, et al., A mathematical model of the solid-polymer-electrolyte fuel cell, J. Electrochem. Soc. 139 (1992) 2477.
[15] T.V. Nguyen, A gas distributor design for proton-exchange-membrane fuel cells, J. Electrochem. Soc. 143 (1996) L103–L105.
[16] E.A. Ticianelli, J.G. Berry, S. Srinivasan, Dependence of performance of solid polymer electrolyte fuel cells with low platinum loading on morphologic characteristics of the electrodes, J. Electroanal. Soc. 135 (9) (1988) 209–2214.